Polarization-dependent Intensity Ratios in Double Resonance Spectroscopy

Kevin K. Lehmann[1]

Departments of Chemistry and Physics, University of Virginia, Charlottesville VA, 22904-4319, USA[a)]

(Dated: 20 September 2023)

Double Resonance is a powerful spectroscopic method that unambiguously assigns the rigorous quantum numbers of one state of a transition. However, there is often ambiguity as to the branch (ΔJ) of that transition. Spectroscopists have resolved this ambiguity by using the dependence of the double resonance intensity on the relative polarization directions of pump and probe radiation. However, published theoretical predictions for this ratio are based upon a weak (i.e. non-saturating) field approximation. This paper presents theoretical predictions for these intensity ratios for cases where the pump field is strongly saturating in the two limits of transitions dominated by homogeneous or of inhomogeneous broadening. Saturation reduces but does not eliminate the magnitude of the polarization effect (driving the intensity ratio closer to unity) even with strong pump saturation. For the case of an inhomogeneously broadened line, such as when Doppler broadened linewidth dominates over]the power-broadened homogeneous line width, a large fraction of the low pump power polarization anisotropy remains. This paper reports predicted polarization ratios for both linear and circular pump and probe field polarizations. The present predictions are compared with experimental measurements on CH_4 ground state $\rightarrow \nu_3 \rightarrow 3\nu_3$ transitions recently reported by de Oliveira *et al.* and these are in better agreement than with the weak field predictions.

[a)]Electronic mail: Lehmann@virginia.edu

I. INTRODUCTION

Double resonance (DR) has long been one of the most powerful methods in the spectroscopist's toolkit.[1] DR is an intrinsically nonlinear spectroscopy that uses two coherent light sources. At least one of these, the pump, creates a nonequilibrium population distribution in a sample, and the other, the probe measures an absorption, emission, scattering, or action spectrum of the resulting nonequilibrium sample. There are three states linked by two transitions.[2]

Using DR greatly simplifies probe spectra[3–12] and, if the pump transition is already assigned, allows the unambiguous assignment of the starting state of probe transitions, which are otherwise difficult to determine when perturbations disrupt regular patterns in the spectra. This disruption is often due to the breakdown of the separation of degrees of freedom, such as vibration and rotation.[13] DR is also useful where homogeneous or inhomogeneous broadening creates substantial overlap between individual transitions. This can result, for example, in a broad rotational contour without resolvable features.[14–18] DR also allows the selective population of states that have negligible thermal populations under available experimental conditions, allowing observation of novel spectroscopic transitions.[19–24] Often, probe transitions reach final states that have only weak or forbidden transitions from the thermally well-populated lower states due to symmetry or propensity selection rules.[25–30]

One can largely eliminate inhomogeneous broadening in DR probe spectra by using narrow bandwidth pump lasers. The pump laser produces a Bennet hole[31] in the velocity distribution of the initial state and a corresponding Bennet hill in the upper state of the pump transition. Probe spectra display sub-Doppler features the widths of which are on the order of the homogeneous widths, which can be orders of magnitude smaller than Doppler broadened widths.[32,33]

DR, especially using a pulsed pump source and a continuous wave (CW) probe field, has been used to study elastic, reorientation, and inelastic collision rates and kernels.[34–42] In addition, Resonant 3-wave mixing, which is another form of DR spectroscopy, has been used to measure enantiomeric excess of chiral molecules[43–46] and to create an enantiomeric excess in single rotational states.[47]

If the common level in the DR scheme is the lowest energy level (called V-type DR), the DR signal is a narrow depletion of the background Doppler Broadened probe transi-

tion. But, if the common level is not the lowest energy state, the pump creates new and narrow absorption (ladder-type DR) or emission features (Λ-type DR) in the probe spectrum, depending upon whether the final state is higher or lower in energy than the pumped (intermediate) state.

The very narrow width of DR transitions can be a drawback when one needs to sample the probe spectrum over a broad spectral range (say 30 THz). The time required to search such a spectral range is on the order of 10 times the detection time constant times the ratio of the scan range divided by the width of the probe DR transitions. Detection of probe transitions of a few MHz or smaller width requires either a very long scan time or a very short detection time constant, which reduces the signal-to-noise ratio (SNR) of the probe spectrum. In addition, the probe spectrum scan must to be repeated for each pump transition studied. The recent demonstration of DR using a stabilized frequency comb for the probe allows one to simultaneously sample the probe spectrum at the frequencies of tens of thousands of comb teeth has dramatically reduced the time required to obtain DR probe spectra over a broad spectral range.[23,24,48]

Selection rules greatly reduce the final states observed in double resonance using a particular pump transition. However, the total angular momentum quantum number, J, of the final state of a probe transition remains ambiguous due to the $\Delta J = 0, \pm 1$ selection rule for dipole transitions. The pump transition produces a nonequilibrium alignment of the angular momentum projection quantum number, M, of the initial and final states,[49]. This alignment produces a probe absorption strength depending on the relative polarization state of the pump and probe fields, which was first reported by Frankel and Steinfeld (1975).[50] The ratio of the DR signal strength with probe wave polarization parallel to that with it perpendicular to the pump wave, gives a polarization ratio that is used to assign the value of ΔJ for the probe transition. One sensitive implementation of DR is polarization spectroscopy, which places nearly crossed polarizers for the pump and probe waves both before and after the sample.[51,52] The pump laser-induced sample dichroism and birefringence results in a change in the transmission of the probe beam that is observed on a greatly reduced background intensity. This results in an increased signal-to-noise ratio when the probe field is dominated by technical intensity noise. Another sensitive variation is polarization modulation where a change in probe transmission is produced by polarization modulation of the pump field.[38,39]

When the pump transition is not saturated, the predicted polarization dependences of the DR signals are easily derived from the dependence of pump and probe field transition intensity on polarization and M. Formulas have been given in the literature[11,25,53–56] but they mostly neglect the effects of optical saturation. Significantly, one optimizes the strength of DR transitions by working with sufficient pump power to have substantial saturation of the pump transition. This produces a larger pump-induced disequilibrium of the sample; predicted polarization ratios in these cases are useful. One of the few cases of the calculation of polarization with strong pumping was published by Spano and Lehmann.[57] They modeled the polarization spectroscopy of a sample that is optically thick for the pump transition. They found that when a strong pulse, of duration substantially shorter than the relaxation time excites a dipole transition, the pulse evolves after propagation into an area-preserving pulse similar to the self-induced transparency of a two-level system.[58] Such a pulse produces an even larger fractional alignment of the sample than that produced by excitation with negligible saturation. However, their analysis is not applicable for DR with continuous wave pump fields, which produce a steady-state response of the sample.[57]

This paper presents an analysis of the polarization dependence of DR signal strength produced by the steady-state response of the sample with and without pump saturation. After the development of the general steady-state case (section IIA), the case of unsaturated pump transitions is developed for the case of linear pump and probe polarization (section IIB). The focus is on the ratio of the DR signal strength with pump and probe fields with parallel over perpendicular polarizations. This is followed by a derivation of the DR intensity ratios when both pump and probe fields are circularly polarized with their electric fields co-rotating divided by counter-rotating (section IIC). This is followed by the cases of saturation of a pump transition dominated by inhomogeneous broadening for both linear and circular polarized fields (section IID). The results for a saturated inhomogeneous broadened pump transition are compared to experimental DR data on CH_4 (section IIE). Lastly, the predicted ratios are derived for cases of a saturation of a homogeneous broadened transition (section IIE). The paper ends with a Summary of the principle results and some conclusions (section III).

II. POLARIZATION DEPENDENCE OF PUMP TRANSITIONS

A. General Steady-State pumping case

Consider a DR signal that results from a pump transition between a pair of levels 1 and 2 and a probe transition between levels 2 and 3, and label the total angular momentum quantum numbers for the three levels as J_1, J_2, and J_3 respectively. Let the pump (probe) transition be driven by waves $a(b)$ with angular frequency and wavevector $\omega_{a,b}$ and $\vec{k}_{a,b}$ respectively. Each J_2, M state will contribute to the DR signal in proportion to its population change caused by the pump laser, $\Delta\rho_{22}(M, \Delta\omega_{12})$. $\Delta\omega_{12}$ is the detuning of the pump from resonance. The J_2, M signal contribution is also proportional to the absorption coefficient of the probe laser by that state, $S(M)$. Both $\Delta\rho_{22}(M, \Delta\omega_{12})$ and $S(M)$ depend upon M and the polarization directions of the pump and probe fields, respectively.

Both pump and probe strengths depend upon the respective transition dipole moment matrix element, which has the form

$$\langle i, M|\vec{\mu}|j, M'\rangle \cdot \hat{G} = \langle i|\mu_g|j\rangle \langle i, M|\phi_{gG}|j, M'\rangle . \tag{1}$$

Here, g specifies the direction of the transition dipole moment, μ, between states i and j in the molecular frame, $\hat{G}$ specifies the direction of the optical electric field, E, in the laboratory fixed frame, and $\langle i, M|\phi_{gG}|j, M'\rangle$ is the direction cosine matrix element, which is the matrix element of $\hat{g} \cdot \hat{G}$. The transition direction cosine matrix elements are given in Table 4.4 of *Microwave Spectroscopy* by Townes and Schawlow[59] and reproduced here in Table I for completeness. The direction cosine matrix elements contain three factors but only the one that depends on J and M for each state, $\phi_G(J, M, J'.M')$ is needed for predicting the polarization dependence – the other two factors are independent of M and the polarization state of the radiation field.

We first consider linear polarization of the pump and probe fields and an initially isotropic sample. The total signals are independent of how we align the laboratory axes; we assign the Z axis as the polarization direction of the pump wave and the Y axis as the propagation direction of both pump and probe fields. With these assignments, we use $\phi_Z(J_1, M, J_2, M)$ for the pump matrix element (as Z axis polarization gives a $\Delta M = 0$ selection rules and, for the probe, $\phi_Z(J_2, M, J_3, M)$ for parallel and $\phi_X(J_2, M, J_3, M \pm 1)$ for perpendicular relative polarizations (as X axis polarization gives a $\Delta M = \pm 1$ selection rule)..

We treat the pump transition as a separate two-level system for each M value. The steady-state change in population in each M state of level 2 can be written in terms of the equilibrium population density difference between levels 1 and 2, $\rho^e_{11}-\rho^e_{22}$; the population and coherence (ρ_{12}) relaxation rates of the pump transition, γ_1, γ_2; the pump Rabi frequency, $\Omega_{12}(M) = \mu_{12}(M)E/\hbar$, where E is the amplitude of the field driving the $1 \leftrightarrow 2$ pump transition; and the detuning from resonance, $\Delta\omega_{12} = \omega_a - \vec{k}_a \cdot \vec{v} - \omega_{12}$ with $\vec{v}$ the velocity of the absorber:[59,60]

$$\Delta\rho_{22}(M, \Delta\omega_{12}) = \frac{(\rho^e_{11} - \rho^e_{22})}{2(2J_2+1)} \frac{(\Omega_{12}(M)^2\gamma_2/\gamma_1)}{\Delta\omega_{12}^2 + \gamma_2^2\,(1 + (\Omega_{12}(M)^2/\gamma_1\gamma_2))}. \tag{2}$$

This describes a power broadened Lorentzian lineshape with half width half maximum (HWHM) of $\gamma_2\sqrt{1 + (\Omega_{12}(M)^2/\gamma_1\gamma_2)}$. We assume that the probe transition is unsaturated, thus for each M value, the absorption strength $S_{23}(M)$is proportional to $\phi_Z(J_2, M, J_3, M)^2$ for $\parallel$ alignment and to $\phi_X(J_2, M, J_3, M+1)^2 + \phi_X(J_2, M, J_3, M-1)^2$ for $\perp$ alignment. The total signal is modeled as the sum over M values of the product $\Delta\rho_{22}(M, \Delta\omega_{12})S_{23}(M)$ and then integrated over any inhomogeneous distribution of transition frequencies. Schwendeman[61,62] pointed out that this is an approximation, but concluded that it holds if one neglects pure M-changing collisions (elastic J-reorientation).

$$\begin{aligned} R_{\text{lin}} &= \frac{I_\parallel}{I_\perp} \qquad (3)\\ &= \frac{\sum_M \int \Delta\rho_{22}(M, \Delta\omega_{12})d\omega_{12})\phi_Z(J_2, M, J_3, M)^2 d\Delta\omega_{12}}{\sum_M \int \Delta\rho_{22}(M, \Delta\omega_{12})d\omega_{12})\left[\phi_X(J_2, M, J_3, M+1)^2 + \phi_X(J_2, M, J_3, M-1)^2\right] d\Delta\omega_{12}}. \end{aligned}$$

If the transition is homogeneously broadened, there is only a single value of $\Delta\omega_{12}$ and thus no integration over detuning.

In most CW gas-phase DR experiments, the pump Rabi frequencies, $\Omega_{12}(M)$, are far below the Doppler width of the pump transition, thus the pump burns a Bennet hole in the velocity distribution of the lower energy state and creates a Bennet hill in the upper energy state. If the pump transition is inhomogeneously Doppler broadened, with lineshape function g_{D} of width $\Delta\omega_{\text{D}} >> \gamma_1, \Omega_{12}(M)$, the integral of Eq. 2 over detuning gives an integrated steady-state population change for level 2

$$\Delta\rho_{22}(M) = \frac{\pi}{2(2J_2+1)}(\rho^e_{11} - \rho^e_{22})g_{\text{D}}(\omega - \omega_{12}) \frac{(\Omega_{12}(M)^2}{\gamma_1\sqrt{1 + (\Omega_{12}(M)^2/\gamma_1\gamma_2)}} \tag{4}$$

B. Unsaturated pump transitions using Linear Polarized pump and probe fields

In the limit of low saturation, $\Omega_{12}^2(M) << \gamma_1\gamma_2$ and Eq.4 reduces to

$$\Delta\rho_{22}(M) \rightarrow \frac{\pi}{2(2J_2+1)}(\rho_{11}^e - \rho_{22}^e)g_{\rm D}(\omega_a - \omega_{12})|\Omega_{12}(M)|^2/\gamma_1. \quad (5)$$

In this limit, the fraction pumped for each M is proportional to Ω_{12}^2 and thus proportional to the intensity and the square of the transition matrix element. In this limit, the absorption coefficient of the probe is

$$\alpha_{23}(\Delta\omega_{23}) = \frac{\omega_{23}}{\epsilon_0 c\hbar}\frac{\gamma_2}{\gamma_2^2+\Delta\omega_{23}^2}\cdot\sum_{M=-J_2}^{J_2}\mu_{23}(M)^2\Delta\rho_{22}(M). \quad (6)$$

Integrating over the probe detuning, we get an integrated absorption coefficient for the unsaturated case:

$$I_G = \int \alpha_{23}d\omega_{23} = \frac{\pi^2\omega_{23}}{(J_2+1)(\epsilon_0 c)^2\hbar^3\gamma_1}(\rho_{11}^e - \rho_{22}^e)g_{\rm D}(\omega-\omega_{12})I_p\cdot\sum_{M=-J_2}^{J_2}\mu_{23}(M)^2\mu_{12}(M)^2. \quad (7)$$

Using the axes assignments given above, for symmetric-top transitions $J_1, K_1, M \rightarrow J_2, K_2, M \rightarrow J_3, K_3, M'$, we have

$$\sum_{M=-J_2}^{J_2}\mu_{23}(M)^2\mu_{12}(M)^2 = \mu_{12}^2\,\mu_{23}^2\,\phi_J(J_1,J_2)^2\phi_g(J_1,K_1,J_2,K_2)^2\phi_J(J_2,J_3)^2\times$$
$$\phi_{g'}(J_2,K_2,J_3,K_3)^2\sum_{M=-J_2}^{J_2}\phi_Z(J_1,M,J_2,M)^2\sum_{M'}\phi_G(J_2,M,J_3,M')^2. \quad (8)$$

In this equation, μ_{12} and μ_{23} are the transition dipole moment matrix elements in the molecular frame for the pump and probe transitions, and $G = Z$ or X depending on whether the probe is polarized parallel to the pump, giving a signal $I_\parallel$, or perpendicular to the pump, giving a signal $I_\perp$. When $G = Z$, the selection rule is $M' = M$, and when $G = X$, the selection rule is $M' = M \pm 1$.

For asymmetric-top molecules, we expand the rotational wavefunction for each state, with quantum numbers i, J_i, τ_i, M as $\phi(i, J_i, \tau_i, M) = \sum_K A(i, J_i, \tau_i, K)\phi_{J_i,K,M}$, where $\phi_{J_1,K,M}$ are symmetric-top wavefunctions. In Eq. 8, we replace the terms

$$\phi_g(J_i, K_i, J_j, K_j)^2 \leftarrow |\sum_{K_i,K_j} A(i, J_i, \tau_i, K_i,)A(j, J_j, \tau_j, K_j)|^2 \phi_g(J_i, K_i, J_j, K_j)|^2. \quad (9)$$

However, these factors cancel in the calculation of the polarization ratio.

The DR signal strength for an arbitrary angle, θ, between pump and probe polarizations is given by

$$I(\theta) = I_{\parallel} \cos^2\theta + I_{\perp} \sin^2(\theta) \quad (10)$$

with

$$I\left(\theta_m = \cos^{-1}(1/\sqrt{3}\right) = (I_{\parallel} + 2I_{\perp})/3. \quad (11)$$

$\theta_m = 54.73^\circ$ is known as the magic angle. The sum

$$\phi_Z(J, M, J', M)^2 + 2\phi_X(J, M, J', M+1)^2 + 2\phi_X(J, M, J', M-1)^2 \quad (12)$$

is M independent and so, at the magic angle of relative polarization, the probe absorption strength is proportional to the total population in the intermediate energy level J_2, K_2. Pure collisional reorientation (M changing collisions), does not impact the DR signal strength with the relative polarization set at the magic angle.

The ratio of $I_{\parallel}$ and $I_{\perp}$ depends only on the sum over M values, as all other factors are independent of pump or probe polarization, thus the polarization ratio in the unsaturated pump case is

$$R_{\rm lin}^{\rm us} = \frac{I_{\parallel}}{I_{\perp}} = \frac{\sum_{M=-J_2}^{J_2} \phi_Z(J_1, M, J_2.M)^2 \phi_Z(J_2, M, J_3, M)^2}{\sum_{M=-J_2}^{J_2} \phi_Z(J_1, M, J_2.M)^2 \left[\phi_X(J_2, M, J_3, M-1)^2 + \phi_X(J_2, M, J_3, M+1)^2\right]}. \quad (13)$$

Given the $\Delta J = 0, \pm 1$ selection rule for both pump and probe transitions, there are 9 possible cases. In each case, the ratio given in Eq. 13 is evaluated using the expressions for ϕ_G given in Table I. The resulting analytical expressions (with sums over M evaluated using Mathematica) are listed in Table II, both in symbolic form and numerical values for $J_2 = 0 - 10$. It is traditional to label molecular transitions with P, Q, R for transitions when J for the upper state minus J for the lower states are equal to $-1, 0, +1$ respectively. These labels change for the three different DR schemes: (ladder-type with $E_1 < E_2 < E_3$, V-type with $E_2 < E_1, E_3$, and Λ-type with $E_2 > E_1, E_3$. Missing entries in the table correspond to dipole-forbidden pump or probe transitions.

	$J' = J+1$	$J' = J$	$J' = J-1$
$\phi(J,J')$	$\left[4(J+1)\sqrt{(2J+1)(2J+3)}\right]^{-1}$	$[4J(J+1)]^{-1}$	$\left[4J\sqrt{(2J-1)(2J+1)}\right]^{-1}$
$\phi_Z(J,M,J',M)$	$2\sqrt{(J+1)^2-M^2}$	$2M$	$2\sqrt{J^2-M^2}$
$(\phi_X \text{ or } \pm\phi_Y)(J,M,J',M\pm1)$	$\mp\sqrt{(J\pm M+1)(J\pm M+2)}$	$\sqrt{(J\mp M)(J\pm M+1)}$	$\pm\sqrt{(J\mp M+1)(J\mp M-1)}$
$\phi_{\rm rms}(J,J')^2$	$\frac{4}{3}(J+1)(2J+3)$	$\frac{4}{3}J(J+1)$	$\frac{4}{3}J(2J-1)$

TABLE I: Table of nonzero direction cosine matrix elements taken from Townes & Schawlow. The symmetric-top matrix element of $< J,K,M|\hat{g}\cdot\hat{h}|J',K',M' >= \phi_(J,J')\phi_g(J,K,J',K')^*\phi_h(J,M,J',M')$ where $\hat{g}$ is the direction of the transition moment in the molecular axis system and $\hat{h}$ is the direction of the electric field in the laboratory fixed axis system. The root mean square values satisfy $\phi^2_{\rm rms} = \sum_{M=-J}^{J}\phi_Z(J,M,J',M)^2/(2J+1) = 2\sum_{M=-J}^{J}\phi_X(J,M,J',M\pm1)^2/(2J+1) = 2\sum_{M=-J}^{J}|\phi_Y(J,M,J',M\pm1)|^2/(2J+1)$

ladder-type	R then R	R then Q	R then P	Q then R	Q then Q	Q then P	P then R	P then Q	P then P
V-type	P then R	P then Q	P then P	Q then R	Q then Q	Q then P	R then R	R then Q	R then P
Λ-type	R then P	R then Q	R then R	Q then P	Q then Q	Q then R	P then P	P then Q	P then R
$J_1 =$	J_2-1	J_2-1	J_2-1	J_2	J_2	J_2	J_2+1	J_2+1	J_2+1
$J_3 =$	J_2+1	J_2	J_2-1	J_2+1	J_2	J_2-1	J_2+1	J_2	J_2-1
J_2	$\frac{4}{3}$	$\frac{2(J_2-1)}{4J_2+1}$	$\frac{8J_2^2+2}{(J_2-1)(6J_2+1)}$	$\frac{2J_2+4}{4J_2+3}$	$\frac{6J_2^2+6J_2-2}{2J_2^2+2J_2+1}$	$\frac{2J_2-2}{4J_2+1}$	$\frac{8J_2^2+16J_2+10}{(J_2+2)(6J_2+5)}$	$\frac{2J_2+4}{4J_2+3}$	$\frac{4}{3}$
0							1.		
1	1.3333	0.	∞	0.8571	2.	0.	1.0303	0.8571	1.3333
2	1.3333	0.2222	2.6154	0.7273	2.6154	0.2222	1.0882	0.7273	1.3333
3	1.3333	0.3077	1.9474	0.6667	2.8000	0.3077	1.1304	0.6667	1.3333
4	1.3333	0.3529	1.7333	0.6316	2.8780	0.3529	1.1609	0.6316	1.3333
5	1.3333	0.3810	1.6290	0.6087	2.9180	0.3810	1.1837	0.6087	1.3333
6	1.3333	0.4000	1.5676	0.5926	2.9412	0.4000	1.2012	0.5926	1.3333
7	1.3333	0.4138	1.5271	0.5806	2.9558	0.4138	1.2151	0.5806	1.3333
8	1.3333	0.4242	1.4985	0.5714	2.9655	0.4242	1.2264	0.5714	1.3333
9	1.3333	0.4324	1.4773	0.5641	2.9724	0.4324	1.2357	0.5641	1.3333
10	1.3333	0.4390	1.4608	0.5581	2.9774	0.4390	1.2436	0.5581	1.3333

TABLE II: Ratio of unsaturated double resonance signal intensity for parallel : perpendicular relative linear polarizations. J_2 is the rotational total angular momentum quantum number for the state common to the two transitions

In the unsaturated limit, the polarization ratios are the same for homogeneously and inhomogeneously broadened cases. We are not aware in the literature of explicit expressions for the predicted DR polarization intensity ratio, $I_{\parallel}/I_{\perp}$, for all cases given in a single reference.. The expressions in Table II can be derived from those previously given in Table 5.1 of the text *Angular Momentum* by Richard Zare,[49]. That table gives the degree of polarization for fluorescence, which is an example of the Λ-type DR scheme but with spontaneous instead of stimulated emission for the probe. Zare gave the polarization anisotropy defined as $P = (I_{\parallel} - I_{\perp})/(I_{\parallel} + I_{\perp})$. The expressions for P were converted to polarization ratios by using $I_{\parallel}/I_{\perp} = (P+1)/(P-1)$ and found to agree with those given in Table II, after correcting for the fact that Zare used what we have written as J_1 in his expressions and we have used J_2. The use of J_2 results in common expressions for all three DR schemes. If the sample is optically thick for the pump, the unsaturated polarization ratio, $R_{\rm lin}$, is unchanged. If the probe transition is optically thick, $R_{\rm lin}$ gives the ratio of the pump field induced change in the probe field absorbance.

C. Unsaturated pump transitions using Circular Polarized pump and probe fields

DR polarization measurement using circular polarizations for the pump and probe fields can be done.[62] In that case, we align the Z axis to the direction of the propagation vectors of the pump and probe fields. The pump and probe fields are assumed to be circularly polarized with positive or negative helicity relative to their respective propagation directions. If the pump and probe fields propagate in the same direction, we define the fields as co-rotating if they have the same helicity and counter-rotating if they have opposite helicity. If they propagate antiparallel, this assignment is reversed; they are co-rotating if they have opposite helicity and counter-rotating if they have the same helicity. The nonzero direction cosine matrix elements of the pump transition are

$$\begin{aligned}\phi_{\pm}(J_1, M, J_2, M \pm 1) &= (\phi_X(J_1, M, J_2, M \pm 1) \pm i\phi_Y(J_1, M, J_2, M \pm 1))/\sqrt{2} \\ &= \sqrt{2}\phi_X(J_1, M, J_2, M \pm 1). \end{aligned} \tag{14}$$

The positive sign is used for absorption from a wave of positive helicity or stimulated emission from a wave of negative helicity. The negative sign is used for absorption from a wave of

negative helicity or stimulated emission from a wave of positive helicity. If the probe co-propagates with the pump, the same signs apply to the probe transition with J_1, J_2 replaced by J_2, J_3. If the probe field counter propagates, we reverse these sign assignments. We can always select the orientation of the Z axis so that the pump transition has a selection rule $J_1, M \rightarrow J_2, M+1$. For ladder DR, we will then have the probe transition a selection rule $J_2, M+1 \rightarrow J_3, M+2$ for co-rotating fields and $J_2, M+1 \rightarrow J_3, M$ for counter-rotating fields. For V-type and λ-type DR, the probe transitions are $J_2, M+1 \rightarrow J_3, M$ for co-rotating fields and $J_2, M+1 \rightarrow J_3, M+2$ for counter-rotating fields. The helicity of a wave is reversed upon normal reflection from a mirror as well as its propagation direction, so the same matrix elements apply for interactions with waves traveling in either direction. As a result, one can use a double pass or even a linear enhancement cavity to increase the DR signal strength assuming that the mirrors have negligible birefringence and dichroism.

We compare the predicted DR signal strength for the cases where the pump and probe electric fields co-rotate or counter-rotate, with signal strengths denoted as I_{same} and I_{opposite} respectively. Using the direction cosine matrix elements, the polarization ratios for ladder DR are calculated to be

$$R_{\text{cir}}^{\text{us}} = \frac{I_{\text{same}}}{I_{\text{opposite}}} = \frac{\sum_{M=-J_2}^{J_2} \phi_X(J_1, M-1, J_2.M)^2 \phi_X(J_2, M, J_3, M+1)^2}{\sum_{M=-J_2}^{J_2} \phi_X(J_1, M-1, J_2, M)^2 \phi_X(J_2, M, J_3, M-1)^2}. \tag{15}$$

As the change in the M quantum number for stimulated emission is opposite that for absorption for fixed helicity, $R_{\text{cir}}^{\text{us}}$ for V-type and Λ-type DR is the inverse of that given in Eq. 15.

Table III gives the predicted non-saturated DR circular polarization ratios. It is evident that circular polarization effects on DR signals are generally larger than for linear polarization effects. In particular, for linear polarization, the predicted ratios for probe transitions with $\Delta J = \pm 1$ approach each other as J increases, making discrimination difficult. For circular polarization, the two $\Delta J = \pm 1$ probe transitions are the most easily distinguished assignments.

Zare's text gives the degree of circular polarization,

$$C(J_1) = \frac{(I_{\text{same}} - I_{\text{opposite}})}{(I_{\text{same}} + I_{\text{opposite}})}, \tag{16}$$

for fluorescence in Table 5.2. Correcting for the inversion for emission vs absorption (equivalently, changing the sign of $C(J_1)$) Zare's expressions were converted and compared to

those given in Table III. The results agree, with the exception of the case that Zare labels ($R\uparrow Q\downarrow$). However, recalculating that $C(J_1)$ value using Zare's eq. 5.124 shows that there was a sign error in his printed table for that entry. With this correction, the two expressions agree.

ladder	R then R	R then Q	R then P	Q then R	Q then Q	Q then P	P then R	P then Q	P then P
V-type	P then R	P then Q	P then P	Q then R	Q then Q	Q then P	R then R	R then Q	R then P
Λ-type	R then P	R then Q	R then R	Q then P	Q then Q	Q then R	P then P	P then Q	P then R
$J_1 =$	J_2-1	J_2-1	J_2-1	J_2	J_2	J_2	J_2+1	J_2+1	J_2+1
$J_3 =$	J_2+1	J_2	J_2-1	J_2+1	J_2	J_2-1	J_2+1	J_2	J_2-1
J_2	6	$\frac{3J_2-3}{3J_2+2}$	$\frac{(J_2-1)(2J_2-3)}{12J_2^2-2}$	$\frac{3J_2+6}{3J_2+1}$	$\frac{(2J_2+3)(2J_2-1)}{4J_2^2+4J_2+2}$	$\frac{3J_2-3}{3J_2+2}$	$\frac{(J_2+2)(2J_2+5)}{12J_2^2+24J_2+10}$	$\frac{3J_2+6}{3J_2+1}$	6.
0							1.		
1	6	0.	0.	2.2500	0.5	0.	0.4565	2.2500	6
2	6	0.3750	0.0217	1.7143	0.8077	0.3750	0.3396	1.7143	6
3	6	0.5455	0.0566	1.5000	0.9000	0.5455	0.2895	1.5000	6
4	6	0.6429	0.0789	1.3846	0.9390	0.6429	0.2617	1.3846	6
5	6	0.7059	0.0940	1.3125	0.9590	0.7059	0.2442	1.3125	6
6	6	0.7500	0.1047	1.2632	0.9706	0.7500	0.2321	1.2632	6
7	6	0.7826	0.1126	1.2273	0.9779	0.7826	0.2232	1.2273	6
8	6	0.8077	0.1188	1.2000	0.9828	0.8077	0.2165	1.2000	6
9	6	0.8276	0.1237	1.1786	0.9862	0.8276	0.2112	1.1786	6
10	6	0.8438	0.1277	1.1613	0.9887	0.8438	0.2069	1.1613	6

TABLE III: Unsaturated double resonance signal polarization ratios for circularly polarized radiation. For ladder double resonance, what is tabulated is the co-rotating / counter-rotating polarization ratios. For V-type and Λ-type DR, what is tabulated is the counter-rotating/ co-rotating polarization ratios. J_2 is the rotational total angular momentum quantum number for the state common to the two transitions

D. Saturated Inhomogeneously Broadened Pump Transitions

In steady-state, saturation of the pump and/or probe transitions generally reduces the polarization effects because it reduces the degree of alignment produced by the pump beam and/or reduces the impact of alignment on the probe absorption. We here consider the case with only saturation of the pump transition.

We start with the case where the inhomogeneous Doppler width is the dominant source of broadening. This is the common situation in continuous wave excitation experiments as it is difficult to achieve a Rabi excitation frequency greater than the Doppler width of the transition, at least for thermal samples at near ambient temperatures or above.

For a strongly saturating pump wave, $\Omega_{12}^2(M) >> \gamma_1\gamma_2$, for all nonzero values of $\mu_{12}(M)$. We again assume that the inhomogeneous Doppler width is substantially larger than Ω_{12}, γ_1, and γ_2. Returning to Eq. 4, taking this limit, and integrating over the detuning gives, for the population change in state 2:

$$\Delta\rho_{22}(M) \rightarrow \frac{\pi}{2(2J_2+1)}(\rho_{11}^e - \rho_{22}^e) g_{\rm D}(\omega_a - \omega_{12})|\Omega_{12}(M)|\sqrt{\gamma_2/\gamma_1)}. \tag{17}$$

The population transferred to level 2 is proportional to $|\Omega_{12}(M)|$ and thus to the square root of the pump intensity. We thus get the following sums for DR transitions $J_1, K_1 \rightarrow J_2, K_2, \rightarrow J_3, K_3$ of symmetric-tops

$$\sum_{M=-J_2}^{J_2} \mu_{23}(M)^2|\mu_{12}(M)| = |\mu_{12}|\,\mu_{23}^2\,\phi_J(J_1,J_2)|\phi_g(J_1,K_1,J_2,K_2)|\phi_J(J_2,J_3)^2 \times$$
$$\phi_{g'}(J_2,K_2,J_3,K_3)^2 \sum_{M=-J_2}^{J_2} |\phi_Z(J_1,M,J_2,M)| \sum_{M'} \phi_G(J_2,M,J_3,M')^2 \tag{18}$$

As above, the case of an asymmetric-top is calculated by replacing the terms

$$|\phi_g(J_i,K_i,J_j,K_j)| \leftarrow |\sum_{K_i,K_j} A(i,J_i,\tau_i,K_i,)A(j,J_j,\tau_j,K_j)|^2 \phi_g(J_i,K_i,J_j,K_j)|. \tag{19}$$

These results lead to the expressions, in the limit of strong pump saturation:

$$I_G^{\rm sat} = \frac{\pi^2\omega_{23}}{2(J_2+1)(\epsilon_0 c)^{3/2}\hbar^2}(\rho_{11}^e - \rho_{22}^e) g_{\rm D}(\omega - \omega_{12})$$
$$sqrt\gamma_2/\gamma_1)\sqrt{2I_p} \cdot \sum_{M=-J_2}^{J_2} \mu_{23}(M)^2|\mu_{12}(M)| \tag{20}$$

and

$$R_{\rm lin}^{\rm sat} = \frac{I_{\parallel}}{I_{\perp}}$$
$$= \frac{\sum_{M=-J_2}^{J_2} \phi_Z(J_1, M, J_2.M)\phi_Z(J_2, M, J_3, M)^2}{\sum_{M=-J_2}^{J_2} \phi_Z(J_1, M, J_2.M)\left[\phi_X(J_2, M, J_3, M-1)^2 + \phi_X(J_2, M, J_3, M+1)^2\right]} \quad (21)$$

$$R_{\rm cir}^{\rm sat} = \frac{I_{\rm same}}{I_{\rm opposite}} = \frac{\sum_{M=-J_2}^{J_2} \phi_X(J_1, M-1, J_2.M)\phi_X(J_2, M, J_3, M+1)^2}{\sum_{M=-J_2}^{J_2} \phi_X(J_1, M-1, J_2, M)\phi_X(J_2, M, J_3, M-1)^2}. \quad (22)$$

Due to the fact that most of the factors $|\phi_Z(J_1, M, J_2, M)|$ and $|\phi_X(J_1, M, J_2, M+1)|$ are square roots of polynomials in J_2 and M, the sums over M values do not lead to compact expressions in the saturated case. The exceptions are the Q pump ratios for linear polarization. However, it is straightforward to numerically calculate the relevant sums for any chosen values of J_1, J_2, and J_3. This was done and the results for linear and circular polarization are presented in tables IV and V, respectively.

In the comparison of the tables for unsaturated and saturated pump conditions, it is evident that, while pump saturation reduces the polarization effects, this reduction is modest and polarization ratios can be used to unambiguously assign transitions. The polarization ratios are independent of the optical depth of the pump transition as long as the steady-state excitation remains strongly saturated throughout the length of the sample.

E. Comparison with Experimental Data

The author and collaborators performed IR-IR double resonance experiments in the spectral range of the CH_4 ground $\rightarrow \nu_3 \rightarrow 3\nu_3$ vibrational transitions.. A CW 3.3 μm Optical Parametric Oscillator generated the pump beam, and a 1.65 μm centered frequency comb the probe beam. The pump transitions were strongly saturated with the pump Rabi frequencies about an order of magnitude larger than the collisional dephasing rate. The results of a preliminary experiment using a single pass, liquid N_2 cooled cell were previously published.[23,24] The newer experiments used an optical cavity for the probe radiation, greatly increasing sensitivity.[63]

Table VI gives a list of double resonance transitions that were observed in this later work. Each transition was measured with both parallel and perpendicular relative polarizations of the pump and probe waves. The probe ΔJ values were assigned based on combination differences and also by comparison with highly accurate theoretical predictions.[64] The observed

ladder	R then R	R then Q	R then P	Q then R	Q then Q	Q then P	P then R	P then Q	P then P
V-type	P then R	P then Q	P then P	Q then R	Q then Q	Q then P	R then R	R then Q	R then P
Λ-type	R then P	R then Q	R then R	Q then P	Q then Q	Q then R	P then P	P then Q	P then R
$J_1 =$	$J_2 - 1$	$J_2 - 1$	$J_2 - 1$	J_2	J_2	J_2	$J_2 + 1$	$J_2 + 1$	$J_2 + 1$
$J_3 =$	$J_2 + 1$	J_2	$J_2 - 1$	$J_2 + 1$	J_2	$J_2 - 1$	$J_2 + 1$	J_2	$J_2 - 1$
J_2				$\frac{2J_2+4}{3J_2+4}$	2.	$\frac{2J_2-2}{3J_2-1}$			
0							1.		
1	1.3333	0.	∞	0.8571	2.	0.	1.0148	0.9282	1.1547
2	1.3244	0.2363	2.5559	0.8000	2.	0.4	1.0449	0.8527	1.1634
3	1.3038	0.3514	1.8494	0.7692	2.	0.5	1.0682	0.8125	1.1690
4	1.2868	0.4194	1.6207	0.7500	2.	0.5455	1.0856	0.7873	1.1703
5	1.2739	0.4640	1.5089	0.7368	2.	0.5714	1.0990	0.7698	1.1759
6	1.2640	0.4954	1.4431	0.7273	2.	0.5882	1.1096	0.7570	1.1783
7	1.2562	0.5187	1.3998	0.7200	2.	0.6000	1.1182	0.7471	1.1802
8	1.2500	0.5365	1.3694	0.7143	2.	0.6087	1.1253	0.7392	1.1817
9	1.2450	0.5507	1.3468	0.7097	2.	0.6154	1.1312	0.7328	1.1830
10	1.2408	0.5621	1.3294	0.7059	2.	0.6207	1.1362	0.7275	1.1842

TABLE IV: Ratio of double resonance signals for parallel over perpendicular relative linear polarization for strongly saturated inhomogeneously broadened pump transitions but unsaturated probe transitions. J_2 is the rotational total angular momentum quantum number for the state common to the two transitions. The first transition listed is the pump' and the 2nd the probe.

and calculated polarization ratios exhibit significant quantitative differences, with observed values systematically closer to unity. Such a bias towards unity can be expected from imperfections in the relative polarization states of the pump and probe lasers in addition to collisional angular momentum reorientation. As that experimental setup no longer exists, we will not speculate on the specific cause(s) of the deviations of the observed and predicted polarization ratios. Never the less, the saturated pump wave predictions are generally closer to the observed values than the unsaturated pump predictions. This demonstrates that even with strong saturation of the pump transitions, which optimizes detection sensitivity, polarization ratios allow for unambiguous assignment of the ΔJ for the observed DR transitions.

ladder	R then R	R then Q	R then P	Q then R	Q then Q	Q then P	P then R	P then Q	P then P
V-type	P then R	P then Q	P then P	Q then R	Q then Q	Q then P	R then R	R then Q	R then P
Λ-type	R then P	R then Q	R then R	Q then P	Q then Q	Q then R	P then P	P then Q	P then R
$J_1 =$	$J_2 - 1$	$J_2 - 1$	$J_2 - 1$	J_2	J_2	J_2	$J_2 + 1$	$J_2 + 1$	$J_2 + 1$
$J_3 =$	$J_2 + 1$	J_2	$J_2 - 1$	$J_2 + 1$	J_2	$J_2 - 1$	$J_2 + 1$	J_2	$J_2 - 1$
$J_2 = 0$							1.		
1	6.	0.	0.	2.25	0.5	0.	0.6531	1.5306	2.4495
2	4.4016	0.4936	0.0479	1.7071	0.8040	0.3876	0.5459	1.3439	2.5777
3	3.8908	0.6628	0.1234	1.4914	0.8967	0.5582	0.4930	1.2549	2.6562
4	3.6454	0.7477	0.1701	1.3761	0.9365	0.6542	0.4614	1.2028	2.7095
5	3.5030	0.7985	0.2005	1.3046	0.9571	0.7159	0.4403	1.1684	2.7482
6	3.4106	0.8323	0.2216	1.2559	0.9691	0.7589	0.4252	1.1440	2.7776
7	3.3461	0.8564	0.2371	1.2206	0.9767	0.7906	0.4139	1.1258	2.8008
8	3.2986	0.8745	0.2489	1.1938	0.9818	0.8149	0.4051	1.1117	2.8195
9	3.2623	0.8885	0.2581	1.1729	0.9854	0.8341	0.3980	1.1004	2.8350
10	3.2337	0.8997	0.2656	1.1560	0.9880	0.8497	0.3922	1.0912	2.8480

TABLE V: Double resonance signal polarization ratios using circularly polarized radiation for strongly saturated inhomogeneously broadened pump transitions but unsaturated probe transitions. For ladder double resonance, what is tabulated is the co-rotating / counter-rotating polarization ratios. For V-type and Λ-type DR, what is tabulated is the counter-rotating/ co-rotating polarization ratios. J_2 is the rotational total angular momentum quantum number for the state common to the two transitions. The first transition listed is the pump; the 2nd the probe.

F. Double Resonance Polarization Ratios for Saturated and Homogeneously Broadened pump transitions

For the sake of completeness, we now treat the case of pump saturation of predominantly homogeneously broadened transitions. As mentioned above, the same polarization ratios are predicted for homogeneously and inhomogeneously broadened unsaturated transitions.

In the homogeneously broadened case, the steady-state $\Delta\rho_{22}(M)$ is proportional to $x(M)/2(1 + x(M))$ with, for linear polarization,

$$x(M) = S\,\phi_Z(J_1, M, J_2, M)^2/\phi_{\rm rms}(J_1, J_2)^2 \tag{23}$$

Pump trans	Probe trans	Wavenumber cm^{-1}	Final Term Value cm^{-1}	Probe Intensity	Polarization Ratio	Saturation Prediction	Unsaturated Prediction
P(2F2)	R(1)	5948.267590(3)	8978.704010(3)	2.26(5)	0.91(4)	1.0148	1.0303
P(2F2)	R(1)	5964.06227(2)	8994.49869(2)	0.081(3)	1.01(7)	1.0148	1.0303
P(2F2)	R(1)	5979.042972(3)	9009.479392(3)	0.56(1)	0.98(4)	1.0148	1.0303
Q(2F2)	Q(2F1)	5928.61142(2)	8978.70401(2)	0.56(3)	1.50(10)	2.0000	2.6154
Q(2F2)	Q(2F1)	5944.40608(2)	8994.49868(2)	0.103(3)	1.55(6)	2.0000	2.6154
Q(2F2)	R(2F1)	5958.673574(6)	9008.766169(6)	2.38(6)	0.83(5)	0.8000	0.7273
Q(2F2)	Q(2F1)	5959.386797(5)	9009.479392(5)	0.89(2)	1.84(7)	2.0000	2.6154
R(2F2)	R(3F1)	5913.18732(2)	8992.78303(2)	0.062(4)	1.1(1)	1.3038	1.3333
R(2F2)	R(3F1)	5918.14141(1)	8997.73712(1)	0.096(4)	1.05(7)	1.3038	1.3333
R(2F2)	R(3F1)	5923.94848(1)	9003.54418(1)	0.44(2)	1.19(6)	1.3038	1.3333
R(2F2)	R(3F1)	5924.26536(2)	9003.86107(2)	0.175(5)	1.10(8)	1.3038	1.3333
R(2F2)	Q(3F1)	5929.170466(3)	9008.766172(3)	4.7(1)	0.44(7)	0.3514	0.3077
R(2F2)	P(3F1)	5929.883687(4)	9009.479393(4)	0.85(2)	1.61(4)	1.8494	1.7333
R(2F2)	R(3F1)	5932.279186(9)	9011.874892(9)	0.100(3)	1.21(9)	1.3038	1.3333
R(2F2)	R(3F1)	5935.245195(3)	9014.840901(3)	0.74(2)	1.36(5)	1.3038	1.3333

TABLE VI: Comparison of observed and predicted polarization intensity ratios for ground state $\rightarrow\ \nu_3\ \rightarrow 3\nu_3$ double resonance transitions of methane. Experimental values are taken from de Oliveria *et al.*[63] The probe intensity is the integrated probe absorption of the sub-Doppler feature in units of 10^{-9} cm^{-2}.

and, for circular polarization,

$$x(M) = 2\,S\,\phi_X(J_1, M, J_2, M)^2/\phi_{\rm rms}(J_1, J_2)^2 \tag{24}$$

S is the saturation parameter, which is the ratio of the pump rate, neglecting saturation, divided by the population relaxation rate, and

$$\phi_{\rm rms}(J_1, J_2)^2 = \sum_{M=-J_2}^{J_2} \phi_Z(J_1, M, J_2, M)^2/(2J_2+1) = 2\sum_{M=-J_2}^{J_2} \phi_X(J_1, M-1, J_2, M)^2/(2J_2+1)$$

Expressions for $\phi_{\rm rms}$ are given in Table I.

Even in the limit of highly saturating pump intensity, the polarization ratios do not go to unity, except for a $J_1 = J_2 + 1$ pump transition, as the selection rules for the $J_1 = J_2$ or $J_2 - 1$ cases prevent pumping all M values of state 2. Below, in tables VII and VIII, the

predicted $S \to \infty$ polarization ratios values for different ΔJ values for the pump and probe transitions are given. In all cases, the high J limit of the highly saturated polarization ratios go to unity, as in that limit, the non-pumped M values represent a negligible fraction of the total.

Figures [1-3] show the linear polarization ratios as a function of S for the three probe transitions when homogeneously broadened $R(5), P(5)$, and $Q(5)$ pump transitions are used. Figures [4-6] show the circular polarization ratios for the same pump transitions. Tables IX and X report the values of the saturation parameter, S, that results in a polarization ratio halfway between the unsaturated and the $S \to \infty$ values for the linear and circular polarization DR experiments respectively, Note that the $J_2 = 1, J_1 = J_3 = 0$ entry is empty for the linear polarization case, because the polarization ratio, in that case, is ∞, independent of S

	$J_2 - J_1 = 1$	$J_2 - J_1 = 0$	$J_2 - J_1 = -1$
$J_3 - J_2 = 1$	$\frac{(2J_2+1)(J_2+3)}{2J_2^2+4J_2+3}$	$\frac{8J_2+10}{8J_2+13}$	1
$J_3 - J_2 = 0$	$\frac{J_2-1}{J_2+2}$	$\frac{4J_2+2}{4J_2-1}$	1
$J_3 - J_2 = -1$	$\frac{J_2+1}{2J_2-2}$	$\frac{2(J_2-1)(4J_2+1)}{8J_2^2-3J_2+1}$	1

TABLE VII: Polarization DR signal ratio, parallel: perpendicularly polarized waves, for a homogeneously broadened pump transition in the limit of saturation parameter $\to \infty$. J_2 is the total angular momentum quantum number of the state common to both transitions.

	$J_2 - J_1 = 1$	$J_2 - J_1 = 0$	$J_2 - J_1 = -1$
$J_3 - J_2 = 1$	$\frac{2J_2^2+7J_2+9}{(J_2(2J_2+1)}$	$\frac{4J_2^2+12J_2+11}{(2J_2+1)(2J_2+1)}$	1
$J_3 - J_2 = 0$	$\frac{(J_2-1)(J_2+3)}{J_2(J_2+2)}$	$\frac{(J_2+2)(2J_2-1)}{(J_2+1)(2J_2+1)}$	1
$J_3 - J_2 = -1$	$\frac{(J_2-1)(2J_2-3)}{J_2(2J_2+1)}$	$\frac{(2J_2-2)}{(2J_2+1)}$	1

TABLE VIII: Polarization ratios, co- : counter-rotating waves, for ladder-type DR signal stengths for Homogeneously broadened pump transition in the limit of saturation parameter $\to \infty$. J is the total angular momentum quantum number of the state common to both transitions. For V-type and Λ-type DR, the ratios should be inverted.

ladder	R then R	R then Q	R then P	Q then R	Q then Q	Q then P	P then R	P then Q	P then P
V-type	P then R	P then Q	P then P	Q then R	Q then Q	Q then P	R then R	R then Q	R then P
Λ-type	R then P	R then Q	R then R	Q then P	Q then Q	Q then R	P then P	P then Q	P then R
$J_1 =$	$J_2 - 1$	$J_2 - 1$	$J_2 - 1$	J_2	J_2	J_2	$J_2 + 1$	$J_2 + 1$	$J_2 + 1$
$J_3 =$	$J_2 + 1$	J_2	$J_2 - 1$	$J_2 + 1$	J_2	$J_2 - 1$	$J_2 + 1$	J_2	$J_2 - 1$
$J_2 = 1$	2.0000	2.0000		1.9541	2.0000	2.0000	0.5502	0.5835	1.2506
2	0.9213	0.9377	0.9030	1.3278	0.9288	1.5002	0.7924	0.8975	1.3969
3	1.1211	1.1877	1.0847	1.7102	1.0027	1.9302	0.9743	1.1458	1.5106
4	1.2688	1.3904	1.2250	1.9762	1.0431	2.206	1.1173	1.3474	1.6015
5	1.3840	1.5583	1.3374	2.1697	1.0703	2.3947	1.2334	1.515	1.676
6	1.4772	1.7001	1.4300	2.3167	1.0904	2.5315	1.3299	1.6568	1.7381
7	1.5544	1.8216	1.5076	2.4321	1.1062	2.6353	1.4116	1.7787	1.7908
8	1.6197	1.9270	1.5739	2.5253	1.1189	2.7167	1.4817	1.8847	1.8361
9	1.6758	2.0195	1.6312	2.6022	1.1294	2.7824	1.5427	1.9779	1.8755
10	1.7245	2.1014	1.6812	2.6666	1.1382	2.8366	1.5962	2.0605	1.9100

TABLE IX: Pump saturation parameter, S, required for the linear polarization ratio to be halfway between unsaturated and the $S \to \infty$ limit

III. SUMMARY AND CONCLUSIONS

This work presents expressions for the predicted changes in DR signal strength as a function of relative pump and probe polarizations. These results are applicable to a wide range of DR experiments performed with the pump population transfer in the steady-state limit. It is found that, even with a strongly saturated pump field, most of the polarization anisotropy is retained in the case of an inhomogeneously broadened pump transition, due to the different power broadened widths of different M projection states. This allows polarization ratios to be used to unambiguously assign the ΔJ values for the probe transitions. Combined with the assignment of the pump transition, this allows determination of the final state term value, symmetry, and total angular momentum quantum numbers for each observed probe transition. The relative polarization dependence is further reduced when a homogeneously broadened transition is strongly saturated. Even there, in most cases, polarization effects remain for low to modest J values due to the fact that not all possible M values of the intermediate state can be pumped.

ladder	R then R	R then Q	R then P	Q then R	Q then Q	Q then P	P then R	P then Q	P then P
V-type	P then R	P then Q	P then P	Q then R	Q then Q	Q then P	R then R	R then Q	R then P
Λ-type	R then P	R then Q	R then R	Q then P	Q then Q	Q then R	P then P	P then Q	P then R
$J_1 =$	$J_2 - 1$	$J_2 - 1$	$J_2 - 1$	J_2	J_2	J_2	$J_2 + 1$	$J_2 + 1$	$J_2 + 1$
$J_3 =$	$J_2 + 1$	J_2	$J_2 - 1$	$J_2 + 1$	J_2	$J_2 - 1$	$J_2 + 1$	J_2	$J_2 - 1$
$J_2 = 1$	2.0000	2.0000	2.0000	1.9541	2.0000	2.0000	0.5502	0.5835	1.2506
2	0.9213	0.9377	0.9030	1.3278	0.9288	1.5002	0.7924	0.8975	1.3969
3	1.1211	1.1877	1.0847	1.7102	1.0027	1.9302	0.9743	1.1458	1.5106
4	1.2688	1.3904	1.2250	1.9762	1.0431	2.2060	1.1173	1.3474	1.6015
5	1.3840	1.5583	1.3374	2.1697	1.0703	2.3947	1.2334	1.5150	1.6760
6	1.4772	1.7001	1.4300	2.3167	1.0904	2.5315	1.3299	1.6568	1.7381
7	1.5544	1.8216	1.5076	2.4321	1.1062	2.6353	1.4116	1.7787	1.7908
8	1.6197	1.927	1.5739	2.5253	1.1189	2.7167	1.4817	1.8847	1.8361
9	1.6758	2.0195	1.6312	2.6022	1.1294	2.7824	1.5427	1.9779	1.8755
10	1.7245	2.1014	1.6812	2.6666	1.1382	2.8366	1.5962	2.0605	1.9100

TABLE X: Pump saturation parameter, S, required for the circular polarization ratio to be halfway between the unsaturated and $S \to \infty$ limits

IV. ACKNOWLEDGEMENTS

The author recognizes Steven L.Coy for conversations on this topic over many years and his and Aleksandra Foltynowicz's encouragement to publish these results. He acknowledges many helpful suggestions on the manuscript, made by Robert Field, which substantially improved the document. He also acknowledges support for the US National Science Foundation.

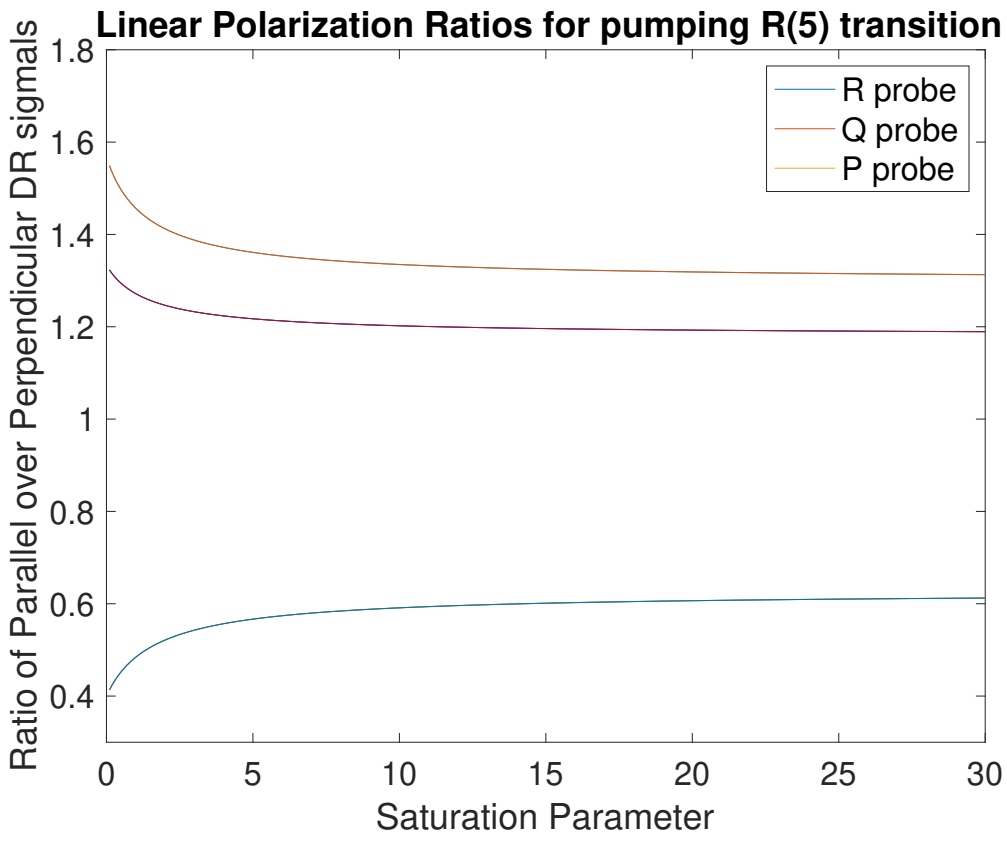

FIG. 1. Probe linear polarization ratios as a function of saturation parameter for R(5) pump transition

REFERENCES

[1]T. Carroll and G. Wolga, IEEE Journal of Quantum Electronics **2**, 456 (1966).

[2]4levelDRnote.

[3]R. Teets, R. Feinberg, T. W. Hansch, and A. L. Schawlow, Physical Review Letters **37**, 683 (1976).

[4]S. L. Coy, K. K. Lehmann, and F. C. Delucia, Journal of Chemical Physics **85**, 4297 (1986).

[5]S. L. Coy and K. K. Lehmann, Journal of Chemical Physics **84**, 5239 (1986).

[6]K. K. Lehmann and S. L. Coy, Berichte Der Bunsen-Gesellschaft-Physical Chemistry Chemical Physics **92**, 306 (1988).

[7]S. L. Coy and K. K. Lehmann, Spectrochimica Acta Part a-Molecular and Biomolecular Spectroscopy **45**, 47 (1989).

[8]K. K. Lehmann and S. L. Coy, Journal of the Chemical Society, Faraday Transactions 2

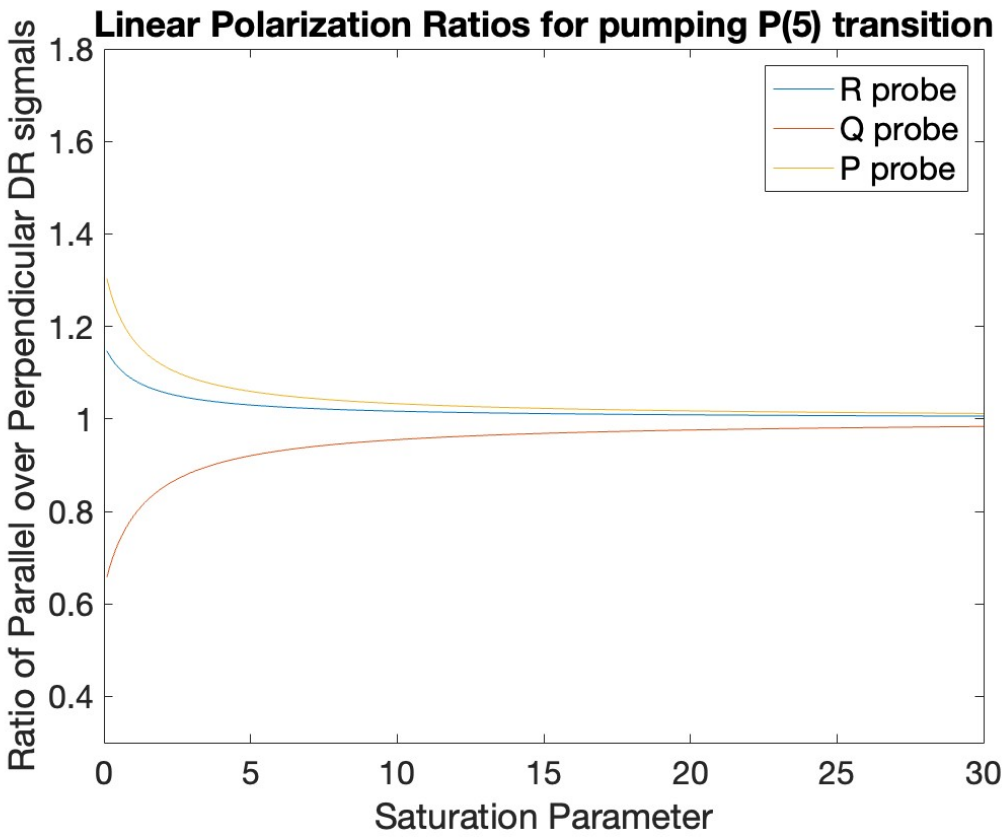

FIG. 2. Probe linear polarization ratios as a function of saturation parameter for P(5) pump transition

84, 1389 (1988).

[9]J. E. Gambogi, E. R. T. Kerstel, K. K. Lehmann, and G. Scoles, Journal of Chemical Physics **100**, 2612 (1994).

[10]J. E. Gambogi, E. R. T. Kerstel, X. M. Yang, K. K. Lehmann, and G. Scoles, Journal of Molecular Spectroscopy **175**, 198 (1996).

[11]M. H. Kabir, S. Kasahara, W. Demtroder, Y. Tatamitani, A. Doi, H. Kato, and M. Baba, Journal of Chemical Physics **119**, 3691 (2003).

[12]R. Zhao, I. M. Konen, and R. N. Zare, The Journal of Chemical Physics **121**, 9938 (2004).

[13]G. B. Park, C. C. Womack, A. R. Whitehill, J. Jiang, S. Ono, and R. W. Field, Journal of Chemical Physics **142**, 12 (2015).

[14]S. A. Henck, M. A. Mason, W. B. Yan, K. K. Lehmann, and S. L. Coy, Journal of Chemical Physics **102**, 4783 (1995).

[15]S. A. Henck, M. A. Mason, W. B. Yan, K. K. Lehmann, and S. L. Coy, Journal of Chemical

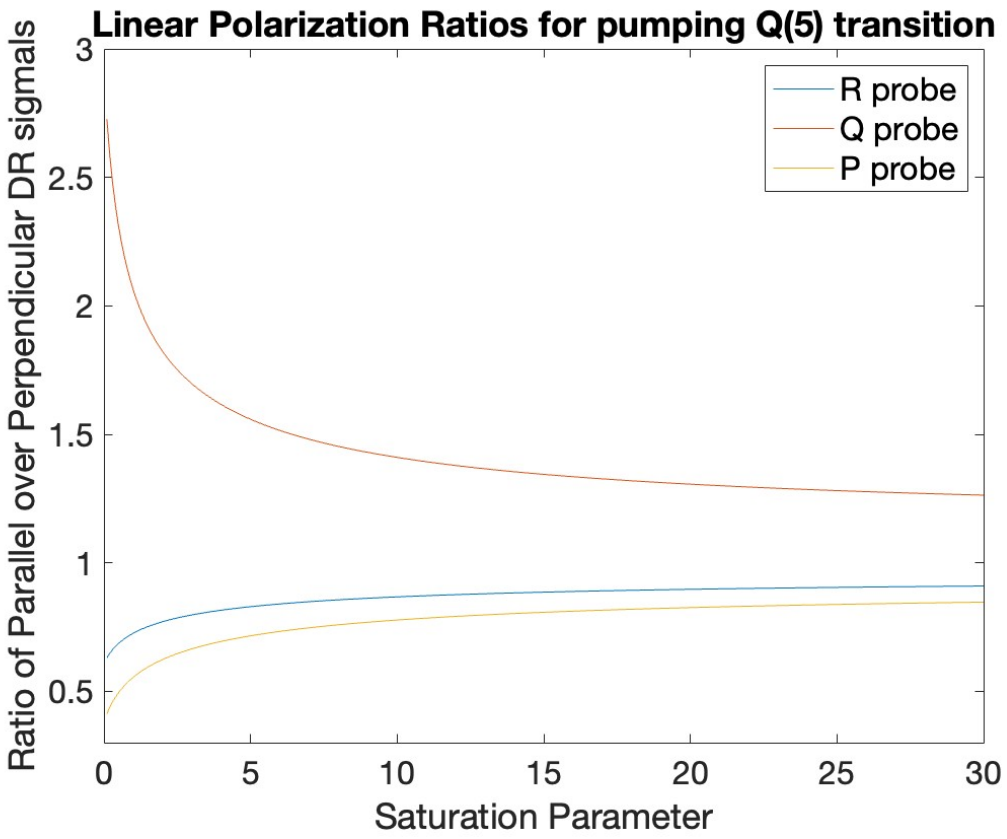

FIG. 3. Probe linear polarization ratios as a function of saturation parameter for Q(5) pump transition

Physics **102**, 4772 (1995).

[16]A. Callegari, H. K. Srivastava, U. Merker, K. K. Lehmann, G. Scoles, and M. J. Davis, Journal of Chemical Physics **106**, 432 (1997).

[17]A. Callegari, U. Merker, P. Engels, H. K. Srivastava, K. K. Lehmann, and G. Scoles, Journal of Chemical Physics **113**, 10583 (2000).

[18]A. Callegari, R. Pearman, S. Choi, P. Engels, H. Srivastava, M. Gruebele, K. K. Lehmann, and G. Scoles, Molecular Physics **101**, 551 (2003).

[19]R. Z. Martinez, K. K. Lehmann, and S. Carter, J Chem Phys **120**, 691 (2004).

[20]T. B. Settersten, R. L. Farrow, and J. A. Gray, Chemical Physics Letters **370**, 204 (2003).

[21]T. Barnum, *Spectroscopy and dynamics of high orbital angular momentum Rydberg states*, Thesis, Massachusetts Institute of Technology (2020).

[22]B. D. Yang, Y. Liu, and J. M. Wang, Optics Communications **474**, 126102 (2020).

[23]A. Foltynowicz, L. Rutkowski, I. Silander, A. C. Johansson, V. Silva de Oliveira, O. Axner,

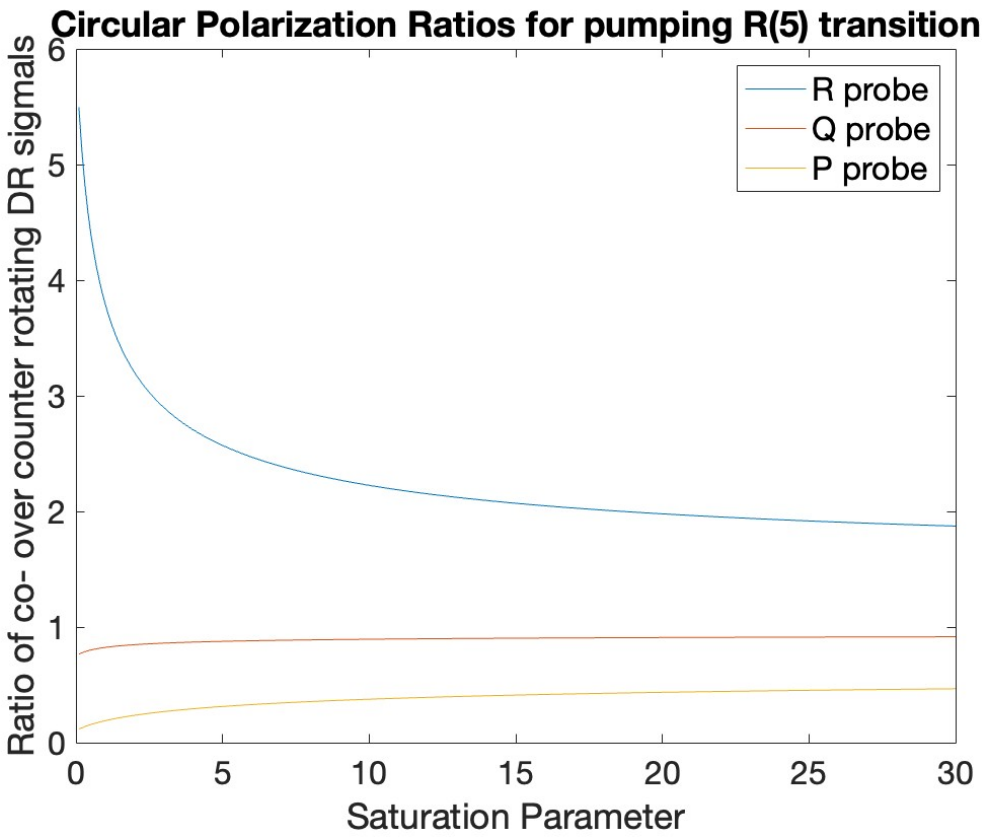

FIG. 4. Probe circular polarization ratios as a function of saturation parameter for R(5) pump transition

G. Sobon, T. Martynkien, P. Mergo, and K. K. Lehmann, Physical Review Letters **126**, 063001 (2021).

[24]A. Foltynowicz, L. Rutkowski, I. Silander, A. C. Johansson, V. S. de Oliveira, O. Axner, G. Sobon, T. Martynkien, P. Mergo, and K. K. Lehmann, Physical Review A **103**, 022810 (2021).

[25]M. Chevalier and A. Demartino, Chemical Physics Letters **135**, 446 (1987).

[26]D. Frye, H. T. Liou, and H. L. Dai, Chemical Physics Letters **133**, 249 (1987).

[27]S. Kasahara, H. Ikoma, and H. Kato, Journal of Chemical Physics **100**, 63 (1994).

[28]S. Kasahara, C. Fujiwara, N. Okada, H. Kato, and M. Baba, Journal of Chemical Physics **111**, 8857 (1999).

[29]H. K. Srivastava, A. Conjusteau, H. Mabuchi, A. Callegari, K. K. Lehmann, and G. Scoles, Review of Scientific Instruments **71**, 4032 (2000).

[30]A. Dia, M. Abboud, P. J. Nacher, and G. Tastevin, European Physical Journal D **75**, 223

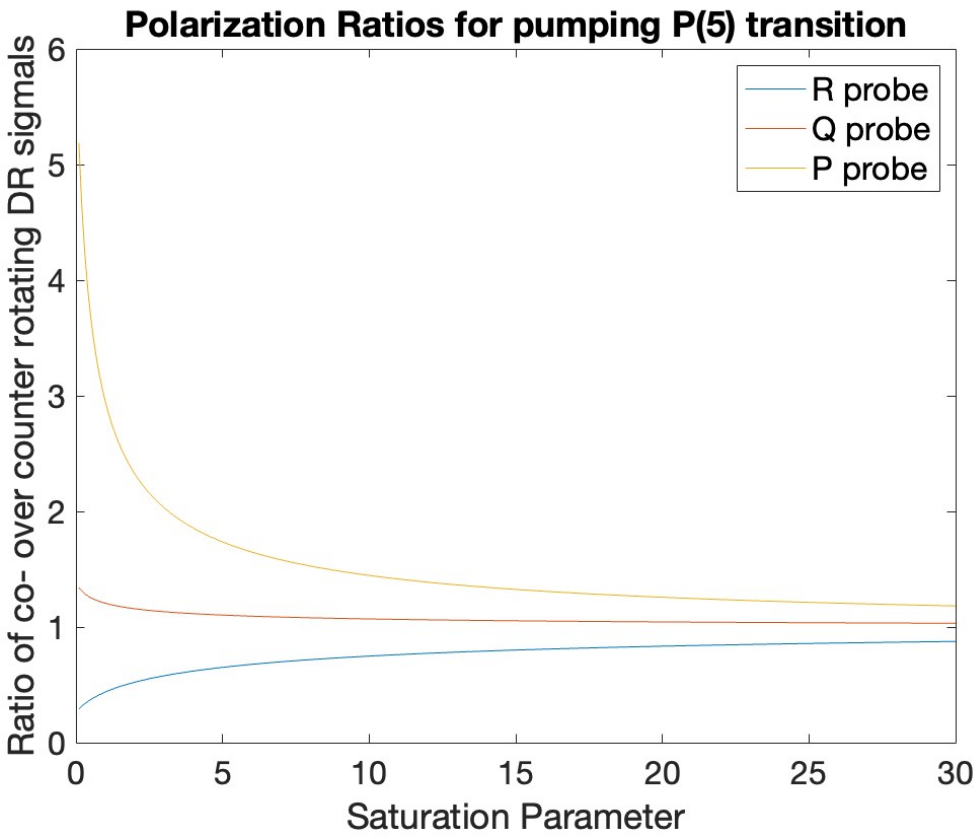

FIG. 5. Probe circular polarization ratios as a function of saturation parameter for P(5) pump transition

(2021).

[31]M. Elbel, M. Simon, and H. Welp, Quantum Optics: Journal of the European Optical Society Part B **2**, 351 (1990).

[32]M. E. Kaminsky, R. T. Hawkins, F. V. Kowalski, and A. L. Schawlow, Physical Review Letters **36**, 671 (1976).

[33]C. Wieman and T. W. Hansch, Physical Review Letters **36**, 1170 (1976).

[34]C. H. Greene and R. N. Zare, The Journal of Chemical Physics **78**, 6741 (1983).

[35]S. L. Coy, S. D. Halle, J. L. Kinsey, and R. W. Field, Journal of Molecular Spectroscopy **153**, 340 (1992).

[36]J. J. Klaassen, S. L. Coy, J. I. Steinfeld, and C. Roche, Journal of Chemical Physics **100**, 5519 (1994).

[37]S. L. Coy, S. D. Halle, J. L. Kinsey, and R. W. Field, Journal of Molecular Spectroscopy **169**, 292 (1995).

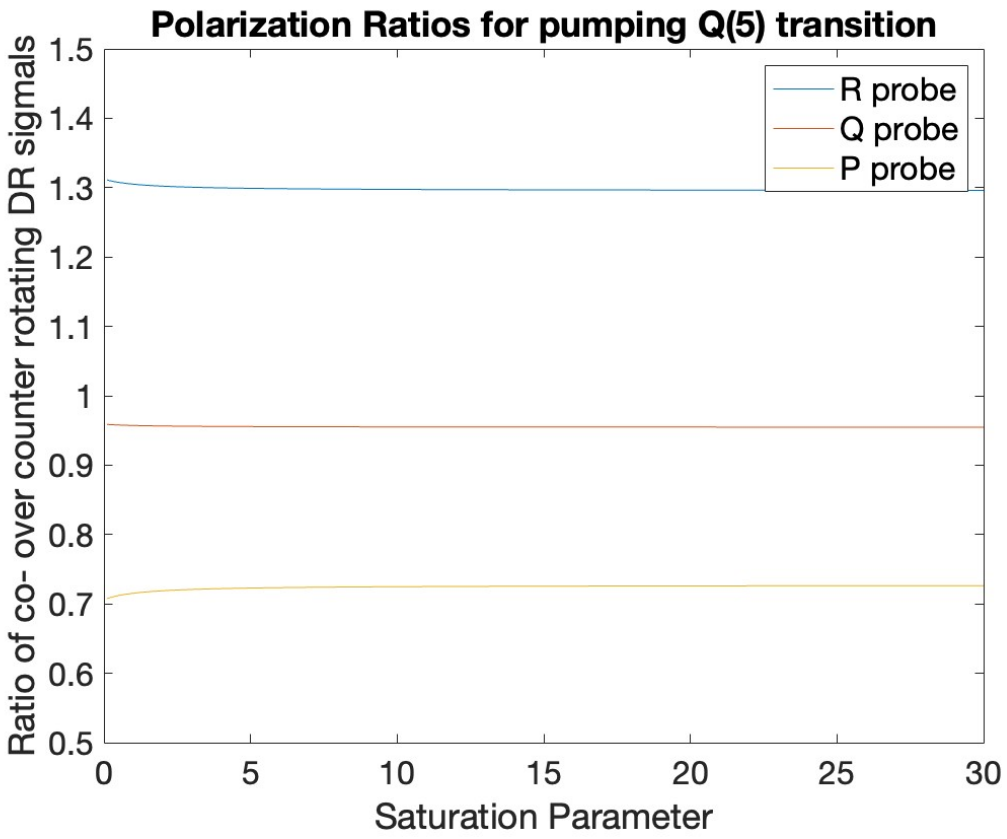

FIG. 6. Probe circular polarization ratios as a function of saturation parameter for Q(5) pump transition

[38]U. Y. Shin and R. H. Schwendeman, Journal of Chemical Physics **96**, 8699 (1992).

[39]G. M. Soriano and R. H. Schwendeman, Journal of Molecular Spectroscopy **190**, 294 (1998).

[40]B. Abel, N. Lange, F. Reiche, and J. Troe, Journal of Chemical Physics **110**, 1389 (1999).

[41]S. B. Bayram, S. Kin, M. J. Welsh, and J. D. Hinkle, Physical Review A **73**, 042713 (2006).

[42]D. Forthomme, M. L. Hause, H. G. Yu, P. J. Dagdigian, T. J. Sears, and G. E. Hall, Journal of Physical Chemistry A **119**, 7439 (2015).

[43]D. Patterson and J. M. Doyle, Physical Review Letters **111**, 023008 (2013).

[44]D. Patterson and M. Schnell, Physical Chemistry Chemical Physics **16**, 11114 (2014).

[45]S. Lobsiger, C. Perez, L. Evangelisti, K. K. Lehmann, and B. H. Pate, Journal of Physical Chemistry Letters **6**, 196 (2015).

[46]K. K. Lehmann, "Theory of enantiomer-specific microwave spectroscopy," in *Frontiers and Advances in Molecular Spectroscopy*, edited by J. Laane (Elsevier, Amsterdam, 2018) Book

section 21, pp. 713–734.

[47]S. Eibenberger, J. Doyle, and D. Patterson, Physical Review Letters **118**, 123002 (2017).

[48]A. Nishiyama, S. Yoshida, Y. Nakajima, H. Sasada, K. Nakagawa, A. Onae, and K. Minoshima, Optics Express **24**, 25894 (2016).

[49]R. N. Zare, *Angular Momentum: Understanding Spatial Aspects in Chemistry and Physics*, 1st ed. (Wiley-Interscience, New York, 1991) p. 368.

[50]D. S. Frankel and J. I. Steinfeld, Journal of Chemical Physics **62**, 3358 (1975).

[51]Z. S. Li, M. Rupinski, J. Zetterberg, Z. T. Alwahabi, and M. Alden, Applied Physics B-Lasers and Optics **79**, 135 (2004).

[52]A. H. Steeves, H. A. Bechtel, S. L. Coy, and R. W. Field, Journal of Chemical Physics **123**, 141102 (2005).

[53]D. M. Jonas, X. Yang, and A. M. Wodtke, The Journal of Chemical Physics **97**, 2284 (1992).

[54]R. Ferber, W. Jastrzebski, and P. Kowalczyk, Journal of Quantitative Spectroscopy & Radiative Transfer **58**, 53 (1997).

[55]K. Chen and E. S. Yeung, The Journal of Chemical Physics **69**, 43 (2008).

[56]V. S. Petrovic and R. W. Field, The Journal of Chemical Physics **128**, 014301 (2008).

[57]F. C. Spano and K. K. Lehmann, Physical Review A **45**, 7997 (1992).

[58]S. L. McCall and E. L. Hahn, Phys. Rev. **183**, 457 (1969).

[59]C. Townes and A. Schawlow, *Microwave Spectroscopy*, 2nd ed. (Dover Books, New York, 2012) p. 720.

[60]R. Karplus and J. Schwinger, Physical Review **73**, 1020 (1948).

[61]R. H. Schwendeman, Journal of Chemical Physics **73**, 4838 (1980).

[62]R. H. Schwendeman, Journal of Molecular Spectroscopy **198**, 129 (1999).

[63]V. S. de Oliveira, I. Silander, L. Rutkowski, G. Sobo?, O. Axner, K. K. Lehmann, and A. Foltynowicz, "Sub-doppler optical-optical double-resonance spectroscopy using a cavity-enhanced frequency comb probe," (2023), preprint available on the Arxiv at webpage https://arxiv.org/abs/2307.03256, arXiv:2307.03256 [physics.chem-ph].

[64]M. Rey, A. Nikitin, B. Bezard, P. Rannou, A. Coustenis, and V. Tyterev, Icarus **303**, 114 (2018).